

Intense Subsurface Upwelling Associated with Major Western Boundary Currents

Fanglou Liao¹, Xinfeng Liang¹, Yun Li¹, and Michael Spall¹

¹University of Delaware

November 24, 2022

Abstract

Western boundary currents (WBCs) play an essential role in regulating global climate. In contrast to their widely examined horizontal motions, less attention has been paid to vertical motions associated with WBCs. Here, we examine the vertical motions associated with the major WBCs by analyzing vertical velocity estimates from five ocean synthesis products and one eddy-resolving ocean simulation. These data reveal robust and intense subsurface upwelling in five major subtropical WBC systems. These upwelling systems are parts of basin-scale zonal overturning circulations and are likely driven by the meridional pressure gradients along the western boundary. The intense subsurface upwelling associated with WBCs and the basin-wide zonal overturning circulations are potentially crucial for the transport of properties and materials in the ocean interior but have long been neglected in the literature. This study suggests an overlooked role of WBCs in the climate system and showcases the usefulness of ocean vertical velocity estimates from various data products.

1 **Intense Subsurface Upwelling Associated with Major Western Boundary Currents**

2 Fanglou Liao¹, Xinfeng Liang^{1*}, Yun Li¹ & Michael Spall²

3 1. School of Marine Science and Policy, University of Delaware, Lewes, DE 19958, USA

4 2. Woods Hole Oceanographic Institution, Woods Hole, MA, 02543, USA

5

6 **Abstract**

7 Western boundary currents (WBCs) play an essential role in regulating global climate¹⁻⁵. In
8 contrast to their widely examined horizontal motions, less attention has been paid to vertical
9 motions associated with WBCs. Here, we examine the vertical motions associated with the major
10 WBCs by analyzing vertical velocity estimates from five ocean synthesis products⁶⁻¹¹ and one
11 eddy-resolving ocean simulation¹². These data reveal robust and intense subsurface upwelling in
12 five major subtropical WBC systems. These upwelling systems are parts of basin-scale zonal
13 overturning circulations^{13, 14} and are likely driven by the meridional pressure gradients along the
14 western boundary. The intense subsurface upwelling associated with WBCs and the basin-wide
15 zonal overturning circulations are potentially crucial for the transport of properties and materials
16 in the ocean interior but have long been neglected in the literature. This study suggests an
17 overlooked role of WBCs in the climate system and showcases the usefulness of ocean vertical
18 velocity estimates from various data products.

19

20 * Corresponding author (email: xfliang@udel.edu)

21 **Introduction**

22 Large-scale vertical motion in the global ocean is generally much weaker than horizontal
23 motions¹⁵, yet vertical transport is crucial in both the climate and biogeochemical systems. For
24 instance, upwelling near the surface brings nutrient-enriched water into the euphotic zone,
25 affecting the ocean primary productivity^{16, 17} and, consequently, CO₂ uptake¹⁸⁻²⁰. Downwelling,
26 such as that observed in the Southern Ocean, transports heat and tracers sourced at the surface to
27 the deep and abyssal oceans²¹⁻²³, and is therefore essential for the responses of the ocean interior
28 to changes in climate and human activities²¹.

29 Based on theoretical understanding (e.g., Ekman dynamics) and the observed distributions of a
30 variety of tracers²⁴, a number of general patterns of ocean vertical motions have been inferred,
31 including strong upwelling along the eastern boundaries of the subtropical ocean basins and
32 along the equator^{17, 25, 26}, as well as intense vertical motions of both signs in the Southern
33 Ocean^{25, 27}. However, because the weak vertical velocity associated with the large-scale
34 circulations cannot, in general, be measured directly with existing instruments, studies of vertical
35 motions are limited, especially in the subsurface ocean. Some available ocean data products,
36 especially ocean state estimates and ocean reanalyses^{28, 29} constrained by observations, provide
37 estimates of ocean vertical velocity. Once proven robust, such data products can complement
38 existing observations and advance our quantitative understanding of large-scale vertical motions
39 in the global ocean.

40 The vertical motions associated with WBCs and their impacts on subsurface vertical exchanges
41 have not been studied widely. Despite the fact that all major WBCs, including the Gulf Stream
42 and Kuroshio, are three-dimensional features, their role in the climate system has long been

43 studied in terms of lateral transport and air-sea exchange³⁰, largely neglecting the effects of
44 vertical motions. In fact, regional observations³¹ and the long-term mean vertical velocity field
45 from a global ocean state estimate³² have revealed considerable vertical motions associated with
46 the WBCs, even in the absence of local upwelling-favorable wind stress. Such WBC-associated
47 vertical motions potentially offer a viable and effective mechanism for the exchange of ocean
48 heat, salt, and other biogeochemical tracers between the upper ocean and the underlying water
49 masses over long timescales.

50 In this study, we examine estimates of vertical velocity in the major WBC regions from one
51 ocean state estimate (ECCO v4r3^{10, 11}), four ocean reanalyses (ECMWF ora-s3⁶; GODAS⁷;
52 SODA 3.4.2⁸; ECDA⁹) and one eddy-resolving ocean simulation (OFES¹²) over their
53 overlapping period (January 1992 to December 2009). Our primary goals are to describe and
54 explain robust large-scale features of vertical motions in the WBC regions and to explore their
55 roles in the vertical transport of water masses and ocean properties. In order to demonstrate
56 differences between vertical motions near eastern and western boundaries of ocean basins, we
57 also include the Peruvian upwelling region as a contrasting example.

58 **Results**

59 **Subsurface vertical velocity associated with the major WBCs.** Time-averaged vertical
60 velocity \bar{w} near 300 m from six selected ocean products is displayed in Fig. 1. While there are
61 differences in the detailed regional patterns, intense vertical motions in the Southern Ocean,
62 along the Equator, and in the WBC regions are observed in all of the examined data products. In
63 contrast to the strong \bar{w} in the Southern Ocean³³ and in the equatorial regions³⁴, which are mainly
64 induced by Ekman dynamics, the strong and robust upwelling (~ 1 m/day) apparent in the WBC

65 regions in all six products is less well understood. Also, both the strength and vertical extent of
66 the upwelling in the WBC regions are distinctly different from those in the eastern boundary
67 upwelling systems, the latter of which are barely detectable at this depth. Strong upwelling can
68 be also seen at 1000 m and deeper in WBC regions, especially near the Gulf Stream and the
69 Kuroshio (Supplementary Figs. 1-2). Apart from the boundary current systems, the vast area of
70 the subtropical oceans at this depth is dominated by weak downwelling.

71 We also present selected sections of the time-averaged vertical velocity \bar{w} across the major
72 WBCs from ECCO (Fig. 2). Despite differences in resolutions, numerical configurations, and
73 assimilated data, all of the examined products show similar spatial patterns (Supplementary Figs.
74 3-8). Intense subsurface upwelling in the WBC regions is collocated with the strong boundary
75 currents, suggesting a dynamical connection between them. Also, the strong time-averaged
76 upwelling (~ 1 m/day) in WBC regions generally extends from near the surface down to 1000 m
77 or even deeper. The strong vertical motion is, however, located well above the bottom
78 topography, suggesting that it does not result from direct interaction with the sloping bottom. In
79 contrast to the WBC sections, upwelling near the Peruvian coast, in a sample eastern boundary
80 upwelling region, is confined to a shallower layer and is also much weaker. Furthermore, weak
81 downwelling with various vertical extents occurs to the east of the WBC upwelling, suggesting
82 possible zonal overturning circulations in the subtropical ocean basins.

83 **Basin-wide zonal overturning and WBC upwelling.** In order to confirm the existence of the
84 zonal overturning circulation suggested above and to examine its relationship with WBC
85 upwelling, we examine the time-averaged velocities in the plane of zonal sections (\bar{u} , \bar{w})
86 averaged within the latitudinal bands marked in Fig. 1b. Zonal overturning circulations are
87 prominent in the North Pacific, North Atlantic and in the Indian Ocean (Fig. 3). Despite

88 differences in detailed structure, all the zonal overturning circulations show weak downward
89 currents inside the ocean basins and strong upwelling near the western boundaries. The intense
90 subsurface upwelling in the WBC regions is, therefore, part of the zonal overturning circulation
91 in the subtropical ocean basins. Note that while this two-dimensional view of a zonal overturning
92 circulation is useful for visualization, it must be kept in mind that the flow is three dimensional³⁵,
93 ³⁶ and time dependent.

94 The existence of zonal overturning circulations in subtropical ocean basins has been
95 demonstrated in previous studies based on idealized numerical simulations^{13, 14}. Meridional
96 gradients in surface buoyancy forcing can drive eastward flows in the upper ocean and westward
97 flows at intermediate depths through the thermal wind balance. Due to mass conservation,
98 upwelling and downwelling are expected at the western and eastern boundaries, respectively, to
99 close the loop. Our analysis shows that similar zonal overturning circulations also exist in
100 realistic settings, as they appear both in a high-resolution realistic numerical simulation (OFES)
101 and in several coarse-resolution ocean synthesis data products. We infer that zonal overturning
102 circulations with upwelling in WBCs are not just theoretical predictions but likely real features
103 of the ocean.

104 In order to seek additional evidence for upwelling in WBC regions, we conduct a few regional
105 analyses. The relationship between the current vectors and the background (zonal) density
106 structure is first examined. Figure 3 shows that velocity vectors in the WBC regions are
107 approximately aligned with sloping isopycnal surfaces associated with the WBCs, suggesting
108 that the strong upwelling in the WBC regions is primarily along rather than across isopycnals. In
109 other words, the strong WBC upwelling is unlikely to be related to local mixing, by which
110 vertical velocity will be primarily in diapycnal direction instead of along isopycnals. A

111 decomposition of the vertical velocity³⁷ from ECCO into diapycnal and isopycnal contributions
112 confirms that the WBC upwelling is mainly associated with along-isopycnal flow
113 (Supplementary Fig. 9). The potential density in the upper 1000 m in the ECCO data increases in
114 the poleward direction along all WBCs (Fig. 4) due to heat loss at the surface and lateral eddy
115 fluxes. The resulting meridional density gradients are balanced by the vertical shear of the zonal
116 velocity (Figs. 2 and 3), as expected from thermal wind. It is this change in stratification along
117 the western boundaries that provides the large-scale constraint for the observed upwelling in the
118 WBCs.

119 The underlying relationship between vertical stratification, horizontal transport, and upwelling is
120 illustrated through a sample volume budget analysis for the Gulf Stream (Fig. 5). The surface
121 area of the control volume is triangular and marked in the inset, and the depth range is between
122 55 m and 2000 m. The budget analysis (Fig. 5a) reveals large horizontal divergences below 300
123 m, requiring vertical transport to conserve mass. The density structure along the two sections
124 (BA, BC in Fig. 5b) provides a dynamical explanation for the existence of horizontal
125 convergence. Since the density increases poleward along the western boundary (Fig. 4), the
126 density change from the western boundary to the interior point (B) is larger along the northern
127 section (BC) than it is along the southern section (AB). Thermal wind thus requires a larger
128 vertical shear in the horizontal velocity along BC. But mass conservation requires that the flow
129 through each section is the same (except for the small transport into the upper 55 m). The only
130 way to close the mass budget is for water to upwell within the control volume. Similar upwelling
131 is found for an idealized high resolution numerical experiment in which a current is cooled with
132 the coast on the left side³⁸. In other words, the WBC upwelling can be explained through mass

133 conservation and geostrophy. The requirement that there be upwelling near the western boundary
134 is not dependent on the details of the numerical model, subgrid mixing, or bottom topography.

135 **Vertical transport associated with the WBC upwelling.** We now quantify the contribution of
136 the WBC upwelling to the vertical transport of mass/volume in the subtropical ocean basins
137 using ECCO (Fig. 6), with the other products generally showing similar results (Supplementary
138 Figs. 3-8). Although the WBC regions occupy only a minor portion of the subtropical ocean
139 basins with respect to the ocean surface area, as shown in Fig. 1b, the vertical volume transport
140 induced by upwelling in the WBCs is generally of the same order of magnitude as and is almost
141 always opposite in the direction to the vertical volume transport in the rest of the subtropical
142 basin within the same latitudinal band. Again, this result is consistent with the conclusion that
143 the WBC upwelling is part of the zonal overturning circulation in the subtropical ocean basins.
144 We also calculate the vertical transport of heat and salt using ECCO (Supplementary Figs. 10-
145 11), and the results are consistent with the volume transport, that the WBC regions dominate
146 subsurface vertical transport of salt and heat in the subtropical ocean basins within certain depth
147 ranges.

148 Specifically, the upwelling in the Kuroshio, Gulf Stream, and Brazil Current regions dominates
149 the net volume transport in the corresponding subtropical ocean basins within the depth ranges
150 between a few hundred and about 2000 m. As a contrasting example, vertical volume transport in
151 the Peruvian upwelling region is much weaker and shallower compared to the WBC upwelling.
152 The net volume transport in the subtropical basin is in general downward near the surface and
153 changes to upward beneath, reflecting the fact that the upward volume transport in the WBCs
154 generally reaches its maximum around 200-500 m. In contrast, the downward transport in the
155 rest of the subtropical basins has its maximum downward volume transport near the surface. The

156 surface intensified downwelling is due to the Ekman pumping occurring inside the subtropical
157 ocean basins and that the maximum impact of the Ekman pumping generally appears around 100
158 m and then decreases significantly with increasing depth, as expected from Sverdrup dynamics.
159 Also, the finding that the zonal overturning circulation is not closed within these latitude bands
160 emphasizes that the WBC upwelling is part of a basin-scale three-dimensional overturning
161 circulation^{35, 36}, part of this upwelling is balanced by downwelling at higher latitudes.

162 We also calculate and compare the vertical volume transport associated with the four major
163 upwelling regimes (WBCs, Eastern Boundary Currents, Equator and Southern Ocean) around the
164 global ocean with ECCO (Fig. 7). Near the surface, equatorial upwelling is the dominant process
165 for the global oceanic vertical volume transport, with a maximum value around 100 Sv. But in
166 the subsurface, the strongest upward transport is associated with the Southern Ocean and the
167 WBC regions. Between 200 m and 1000 m, the WBC-related upward volume transport is
168 generally more than 1/3 of the value in the Southern Ocean, with the maximum value around 25
169 Sv appearing near 400 m. Below 2000 m the pressure gradient along the western boundary is
170 weak and thus a reduced contribution to the upward transport is expected. Again, this
171 comparison confirms that the overlooked role of the WBC upwellings in the subsurface vertical
172 exchanges of ocean properties and materials.

173 **Discussion**

174 To the best of our knowledge, this is the first study providing convincing evidence for the
175 existence of as well as a dynamical explanation for intense subsurface upwelling associated with
176 the major WBCs around the global ocean. Vertical motions in many regions of the global ocean,
177 such as in Eastern Boundary Currents, along the Equator, and in the Southern Ocean, show

178 evident upwelling signals in surface temperature and/or chlorophyll fields^{17, 24-27, 39} and have
179 been known and studied for a long time. In contrast, vertical motions in WBC regions are
180 generally weak at the surface and only become strong below the surface. Also, the strong
181 horizontal transport and eddies associated with WBCs make direct detection of surface signals of
182 WBC upwelling challenging. The intense subsurface upwelling in WBC regions, therefore, have
183 long been unrecognized in the literature.

184 Although in this study subsurface upwelling in the WBC regions is not directly measured but
185 from a variety of ocean data products, there is evidence supporting the inference that WBC
186 upwelling is likely a real phenomenon in the global ocean. The primary reason we believe that
187 the WBC upwelling is real is that in order for the western boundary currents to remain in
188 geostrophic balance to leading order, the observed density gradient along the western boundary
189 requires that there be upwelling. Secondly, the WBC subsurface upwelling appears in all the
190 examined products (Supplementary Figs. 3-8), including coarse-resolution ocean synthesis
191 products and a high-resolution ocean model simulation. Those products differ in many aspects,
192 including ocean model numerics, external forcing, mixing parameterizations and assimilated
193 observational data. The apparent robustness of WBC upwelling suggests that it is likely
194 controlled by a mechanism that is well represented in all the products. Thirdly, vertical motions
195 in other regions of the global ocean (e.g., at low latitudes, and in eastern boundary currents) in
196 the examined data products are generally consistent with previous theoretical and observational
197 studies, further increasing our confidence in their representation of the large-scale vertical
198 motions. Finally, previous idealized theoretical and numerical model studies suggest the
199 existence of zonal overturning circulations in the subtropical ocean basins. Although this aspect
200 has never been explicitly examined, those zonal overturning circulations have upwelling

201 branches near the western boundaries. Our finding of subsurface WBC upwelling is therefore
202 consistent with the predictions of those prior studies.

203 This basic mechanism of the WBC upwelling is analogous to the dynamics of the downwelling
204 limb of the buoyancy-forced meridional overturning circulation^{38, 40}, where the Eulerian
205 downwelling is located in regions of density gradients along the boundary. Eddies contribute an
206 important buoyancy flux which allows parcels to flow along rising isopycnals while the mean
207 Eulerian transport would imply a large downward diapycnal flux^{40, 41}. We expect that eddies may
208 also be important in WBCs but anticipate a lesser role than in downwelling regions because the
209 Eulerian vertical velocity is of the same sign as the flow along rising isopycnals whereas for
210 downwelling they are of opposite sign.

211 Since vertical motions in the WBC regions can reach much deeper than in equatorial and Eastern
212 Boundary upwelling, and may also extend upward into the surface mixed layer, they can play an
213 important role in the subsurface exchange of ocean properties and materials and air-sea exchange
214 in the subtropical regions. Given the consistent and strong vertical motions, the vertical transport
215 of heat and carbon in the WBCs may be significant in regulating the heat and carbon content in
216 both the upper ocean and atmosphere over longer timescales. Moreover, the basin-wide zonal
217 overturning circulations in the subtropical ocean basins could exchange ocean properties and
218 tracers between the ocean interior and western boundaries, as well as playing a role in the
219 climate system.

220 Our results showcase the use of estimates of ocean vertical velocity. While point-wise estimates
221 of ocean vertical velocity from models and reanalysis products are generally weak and noisy,
222 spatial filtering reveals interesting and robust large-scale patterns that are not readily apparent in

223 other variables. We consider it particularly surprising that we have been able to determine a
224 novel aspect of WBCs, one of the most widely studied ocean processes, simply by examining
225 estimates of time-averaged vertical velocity from available ocean synthesis and modeling
226 products. At present, few ocean synthesis products and climate models provide output of ocean
227 vertical velocity, which we suggest should be archived routinely.

228

229 **Methods**

230 **Data.** Estimates of vertical velocity from six publicly available datasets, including one ocean
231 state estimate, four ocean reanalyses, and one eddy-resolving ocean simulation, were analyzed in
232 this study. Some basic information on those datasets is provided in the following. The ECCO
233 (Estimating the Circulation and Climate of the Ocean) data utilized in this study are the
234 ECCOv4r3 monthly estimates^{10, 11}; ECDA is the Ensemble Coupled Data Assimilation System
235 developed at the Geophysical Fluid Dynamics Laboratory⁹; ECMWF used here is ECMWF ora-
236 s3, an operational ocean analysis/reanalysis system implemented at the ECMWF (European
237 Centre for Medium-Range Weather Forecasts⁶); GODAS is the Global Ocean Data Assimilation
238 operated at the National Centers for Environmental Prediction⁷; SODA used here is the version 3
239 of the Simple Ocean Data Assimilation that is based on the ocean component of the coupled
240 CM2.5 model maintained at NOAA/GFDL⁸, and the SODA data we used are monthly
241 interpolated values; OFES is an eddy-resolving quasi-global ocean model developed by the
242 Japan Agency for Marine-Earth Science and Technology¹².

243 For consistency, all available vertical velocity estimates from the six products were transformed
244 to the LLC90¹⁰ (Lat-Lon-Cap 90) grid before further processing. A 3 grids \times 3 grids smoothing

245 filter included in the `gcmfaces`¹⁰ package was applied to obtain robust large-scale patterns. Other
246 smoothing filters (2×2 , 4×4) were also tested, and the results were roughly the same.

247 Additional information about the data products can be found in the Supplementary Table 1.

248 **Domain of the WBC and Peruvian upwelling regions.** As shown in Fig 1a, we define a box
249 for each subtropical WBC region and for the Peruvian upwelling region. The regions covered by
250 those boxes are as follows: Kuroshio, (120°E, 28°N) to (150°E, 40°N); Gulf Stream, (82°W,
251 25°N) to (60°W, 41°N); Agulhas Current, (20°E, 37°S) to (38°E, 27°S); East Australian Current,
252 (148°E, 37°S) to (158°E, 20°S); Brazil Current, (56°W, 35°S) to (30°W, 10°S); Peruvian
253 upwelling, (85°W, 40°S) to (70°W, 8°S).

254 **Global distribution of time-averaged vertical velocity \bar{w} .** The overlapping period covered by
255 all six products is from Jan 1992 to Dec 2009. The vertical velocity data were averaged over this
256 18-years period. We include three sample layers (50 m, 300 m, and 1000 m) here and show the
257 layer around 300 m in the main text and the other two layers in the supplementary information.
258 For each of the six data products, we use the vertical layer closest to the three nominal depths.

259 **Vertical structure of time-averaged vertical motions in WBCs.** For each WBC region, we
260 choose a cross section approximately perpendicular to the local coastline and plot the distribution
261 of time-averaged vertical velocity along with the horizontal velocity that is in the plane of the
262 cross section. Details of the selected cross sections are as follows: Kuroshio, (139°E, 35°N) to
263 (149°E, 25°N); Gulf Stream, (74°W, 38°N) to (64°W, 28°N); Agulhas Current, (30°E, 31°S) to
264 (40°E, 41°S); East Australian Current, (153°E, 30°S) to (163°E, 30°S); and Brazil Current,
265 (41°W, 21°S) to (31°W, 21°S). A contrasting eastern boundary upwelling, the Peruvian upwelling

266 region, was also selected from (70°W, 23°S) to (80°W, 23°S). The cross sections are marked in
267 Fig. 1a.

268 **Zonal overturning circulation.** For the domains represented by the black boxes in Fig. 1b, we
269 calculate meridionally averaged vertical and zonal velocities, which are normalized to the
270 regional horizontal and vertical maxima, respectively, for better visualization. The maxima of
271 depth in each longitude line within the box is added, taken from the General Bathymetric Chart
272 of the Oceans, is shown in Fig. 3.

273 **Vertical velocity decomposition.** Vertical velocity at the sample depth (300 m) is decomposed
274 into isopycnal and diapycnal components following previous studies³⁷. Firstly, potential density
275 is calculated with temperature and salinity data from ECCO; secondly, the horizontal isopycnal
276 slopes in the east-west and north-south directions are calculated; thirdly, isopycnal velocity is
277 calculated by using the continuity equation in density coordinates, and diapycnal velocity is
278 calculated based on the principle that the diapycnal mixing contributes to the advective part of
279 any potential density sources in the diapycnal direction.

280 **Volume budget analysis.** We choose the Gulf Stream region as an example and calculate the
281 horizontal time-averaged volume transport at the two lateral sides and also the time-averaged
282 vertical volume transport through the upper and bottom surfaces. The depths of the upper and
283 bottom surfaces are chosen so that the vertical volume transport at the upper surface is below the
284 Ekman layer and that at the bottom surface is relatively weak. Note that the ECCO data on the
285 native grid are used for the budget analysis.

286 **Vertical volume, heat and salt transport.** At each depth layer, we select the grids with positive
287 mean vertical velocity and calculate the upward vertical volume flux in the domain bounded by

288 each box in Fig. 1a. We define the results as the vertical volume transport related to the WBC
289 upwelling. We also calculate the volume transport within all the other grid cells in the same
290 latitude band across the whole ocean basin (domain shown in Fig. 1b). The sum of these two
291 terms is the net volume transport within the corresponding latitude band across the ocean basin.
292 The vertical heat flux is obtained by multiplying the vertical velocity with specific heat and
293 temperature at each grid, and then integrating in the same way as the volume transport. Note that
294 we use normalized temperature by dividing the temperature of each grid by the global mean
295 temperature in the corresponding vertical layer, to account for the large vertical gradient in
296 temperature. To calculate the vertical salt transport, we multiply the vertical velocity with
297 salinity at each grid and integrate them in the same way as for the vertical volume transport.

298 **Comparison of the vertical volume transport associated with different upwelling regimes.**

299 We calculate the vertical volume transport at each grid where the time-averaged vertical velocity
300 is positive in all the four different regimes: WBC, Eastern Boundary Current, Equator (within 8°
301 equator toward) and the Southern Ocean (south to 40°S). Note that the Angola Dome is
302 classified into the eastern boundary current region in this paper. These upward volume transports
303 are then summed over the corresponding region and compared with each other.

304

305 **Code availability.** The scripts used to make the plots in this paper are available from the
306 corresponding author on request.

307 **Data Availability.** All the data used in this study are publicly available. The ECCOv4r3 data are
308 available at <https://ecco.jpl.nasa.gov/products/all/>. The ECDA data are available at
309 <ftp://nomads.gfdl.noaa.gov/2/ECDA/ecda/GFDL-CM2.1-ECDA/CM2.1R-ECDA-v3.1->

310 1960/mon/ocean/dc_Omon/r1i1p1/v20110601/. The ECMWF data are available at
311 http://apdrc.soest.hawaii.edu:80/dods/public_data/
312 Reanalysis_Data/ORA-S3/1x1_grid. The GODAS data are available at
313 http://apdrc.soest.hawaii.edu:80/dods/public_data/Reanalysis_Data/GODAS/monthly. The
314 SODA data are available at [https://www.atmos.umd.edu/~ocean/index_files/](https://www.atmos.umd.edu/~ocean/index_files/soda3.4.2_mn_download_b.htm)
315 [soda3.4.2_mn_download_b.htm](https://www.atmos.umd.edu/~ocean/index_files/soda3.4.2_mn_download_b.htm). The OFES data are available at
316 http://www.jamstec.go.jp/esc/fes/dods/OFES/OFES_NCEP_RUN. The bathymetry data are
317 available at https://www.gebco.net/data_and_products/gridded_bathymetry_data/.
318

319 **Reference**

- 320 1. Stommel, H.M. The Gulf Stream. A Physical and Dynamical Description. (Cambridge
321 University Press, 1965)
- 322 2. Imawaki, S., Bower, A. S., Beal, L. & Qiu, B. Western boundary currents. *Ocean*
323 *Circulation and Climate - A 21st Century Perspective*. G. Siedler et al., Eds., Academic
324 Press. **103**, 305-338 (2013).
- 325 3. Minobe, S., et al. Influence of the Gulf Stream on the troposphere. *Nature* **452**, 206-209
326 (2008).
- 327 4. Takahashi, T., et al. Climatological mean and decadal change in surface ocean pCO₂, and
328 net sea–air CO₂ flux over the global oceans. *Deep-Sea Res. Part II: Topical Studies in*
329 *Oceanography* **56**, 554-577 (2009).
- 330 5. Wu, L., et al. Enhanced warming over the global subtropical western boundary currents.
331 *Nat. Climate Change* **2**, 161-166 (2012).
- 332 6. Balmaseda, M.A., Vidard, A. & Anderson, D.L. The ECMWF ocean analysis system:
333 ORA-S3. *Mon. Weather. Rev.* **136**, 3018-3034 (2008).
- 334 7. Behringer, D. & Xue, Y. Evaluation of the global ocean data assimilation system at NCEP:
335 The Pacific Ocean. *Proc. Eighth Symp. on Integrated Observing and Assimilation Systems*
336 *for Atmosphere, Oceans, and Land Surface*. 2004. AMS 84th Annual Meeting, Washington
337 State Convention and Trade Center.

- 338 8. Carton, J.A., Chepurin, G.A. & Chen, L. SODA3: A new ocean climate reanalysis. *J. Clim.*
339 **31**, 6967-6983 (2018).
- 340 9. Chang, Y.-S., et al. An assessment of oceanic variability for 1960–2010 from the GFDL
341 ensemble coupled data assimilation. *Clim. Dyn.* **40**, 775-803 (2013).
- 342 10. Forget, G., Campin, J.M., Heimbach, P., Hill, C.N., Ponte, R.M. and Wunsch, C. ECCO
343 version 4: an integrated framework for non-linear inverse modeling and global ocean state
344 estimation, *Geosci. Model Dev.*, **8**, 3071–3104 (2015)
- 345 11. Fukumori, I., et al. ECCO version 4 release 3. <http://hdl.handle.net/1721.1/110380> (2017).
- 346 12. Sasaki, H., et al.. An eddy-resolving hindcast simulation of the quasiglobal ocean from 1950
347 to 2003 on the Earth Simulator. *High resolution numerical modelling of the atmosphere and*
348 *ocean*. 157-185 (2008).
- 349 13. Bryan, F. Parameter sensitivity of primitive equation ocean general circulation models. *J.*
350 *Phys. Oceanogr.* **17**, 970-985 (1987).
- 351 14. Cessi, P., Wolfe, C.L. & Ludka, B.C. Eastern-boundary contribution to the residual and
352 meridional overturning circulations. *J. Phys. Oceanogr.* **40**, 2075-2090 (2010).
- 353 15. Stewart, R.H. Introduction to physical oceanography. 2008: Texas A & M University
354 College Station.
- 355 16. Ryther, J.H. Photosynthesis and fish production in the sea. *Science* **166**, 72-76 (1969).
- 356 17. Kämpf, J. & Chapman, P. Upwelling systems of the world. 2016: Springer.

- 357 18. Ducklow, H.W., Steinberg, D.K. & Buesseler, K.O. Upper ocean carbon export and the
358 biological pump. *Oceanography* **14**, 50-58 (2001).
- 359 19. Pilskaln, C.H., et al. Carbon export and regeneration in the coastal upwelling system of
360 Monterey Bay, central California. *J. Mar. Res.* **54**, 1149-1178 (1996).
- 361 20. Stukel, M.R., et al. Contributions of mesozooplankton to vertical carbon export in a coastal
362 upwelling system. *Mar. Ecol. Prog. Ser.* **491**, 47-65 (2013).
- 363 21. Gregory, J.M. Vertical heat transports in the ocean and their effect on time-dependent
364 climate change. *Clim. Dyn.* **16**, 501-515 (2000).
- 365 22. Ito, T., Woloszyn, M. & Mazloff, M. Anthropogenic carbon dioxide transport in the
366 Southern Ocean driven by Ekman flow. *Nature* **463**, 80–83 (2010).
- 367 23. Liang, X., et al. Vertical redistribution of oceanic heat content. *J. Clim.* **28**, 3821-3833
368 (2015).
- 369 24. Toggweiler, J., et al. Upwelling in the ocean basins north of the ACC: 1. on the upwelling
370 exposed by the surface distribution of $\Delta^{14}\text{C}$. *J. Geophys.*
371 *Res. -Oceans.* **124**, 2591-2608 (2019).
- 372 25. Huyer, A. Coastal upwelling in the California Current system. *Prog. Oceanogr.* **12**, 259-284
373 (1983).
- 374 26. Wyrki, K. An estimate of equatorial upwelling in the Pacific. *J. Phys. Oceanogr.* **11**, 1205-
375 1214 (1981).

- 376 27. Marshall, J. & Speer, K. Closure of the meridional overturning circulation through Southern
377 Ocean upwelling. *Nat. Geosci.* **5**, 171-180 (2012).
- 378 28. Stammer, D., et al. Ocean data assimilation in support of climate applications: status and
379 perspectives. *Ann. Rev. Mar. Sci.* **8**, 491-518 (2016).
- 380 29. Balmaseda, M.A., et al. The ocean reanalyses intercomparison project (ORA-IP). *J. Oper.*
381 *Ocenograph.* **8**, S80-S97 (2015).
- 382 30. Hu, D., et al. Pacific western boundary currents and their roles in climate. *Nature* **522**, 299-
383 308 (2015).
- 384 31. Roughan, M. and Middleton, J.H. On the East Australian Current: variability,
385 encroachment, and upwelling. *J. Geophys. Res. -Oceans.* **109**, C7 (2004).
- 386 32. Liang, X., Spall, M. & Wunsch, C. Global ocean vertical velocity from a dynamically
387 consistent ocean state estimate. *J. Geophys. Res. -Oceans.* **122**, 8208-8224 (2017).
- 388 33. Anderson, R., et al. Wind-driven upwelling in the Southern Ocean and the deglacial rise in
389 atmospheric CO₂. *Science* **323**, 1443-1448 (2009).
- 390 34. Yoshida, K. A Theory of the Cromwell current (the equatorial undercurrent) and of the
391 equatorial upwelling: an interpretation in a similarity to a coastal circulation. *日本海洋学会*
392 *誌* **15**, 159-170 (1959).
- 393 35. Talley, L.D. Shallow, intermediate, and deep overturning components of the global heat
394 budget. *J. Phys. Oceanogr.* **33**, 530-560 (2003).

- 395 36. Boccaletti, G., et al. The vertical structure of ocean heat transport. *Geophys. Res. Lett.* **32**,
396 L10603, doi:10.1029/2005GL022474 (2005).
- 397 37. Bennett, S.L. The relationship between vertical, diapycnal, and isopycnal velocity and
398 mixing in the ocean general circulation. *J. Phys. Oceanogr.* **16**, 167-174 (1986).
- 399 38. Katsman, C.A., et al. Sinking of dense north atlantic waters in a global ocean model:
400 location and controls. *J. Geophys. Res. -Oceans.* **123**, 3563-3576 (2018).
- 401 39. Naveira Garabato, A.C., et al. High-latitude ocean ventilation and its role in Earth's climate
402 transitions. *Phil. Trans. R. Soc. A.* **375**, 20160324 (2017).
- 403 40. Spall, M.A. Buoyancy-forced downwelling in boundary currents. *J. Phys. Oceanogr.*, **38**,
404 2704-2721 (2008).
- 405 41. Cessi, P. & Wolfe, C.L. Adiabatic eastern boundary currents. *J. Phys. Oceanogr.* **43**, 1127-
406 1149 (2013).
- 407
- 408

409 **Acknowledgments**

410 X.L. is supported by the National Science Foundation through Grant OCE-2021274 and the
411 Alfred P. Sloan Foundation through Grant FG-2019-12536. M.A.S is supported through the
412 National Science Foundation Grant OCE-1947290. Comments from Carl Wunsch, Young-Oh
413 Kwon and Jinbo Wang on an early version of this paper are helpful. We also greatly appreciate
414 comments and edits from Andreas Thurnherr on various versions of this paper.

415

416 **Author contributions**

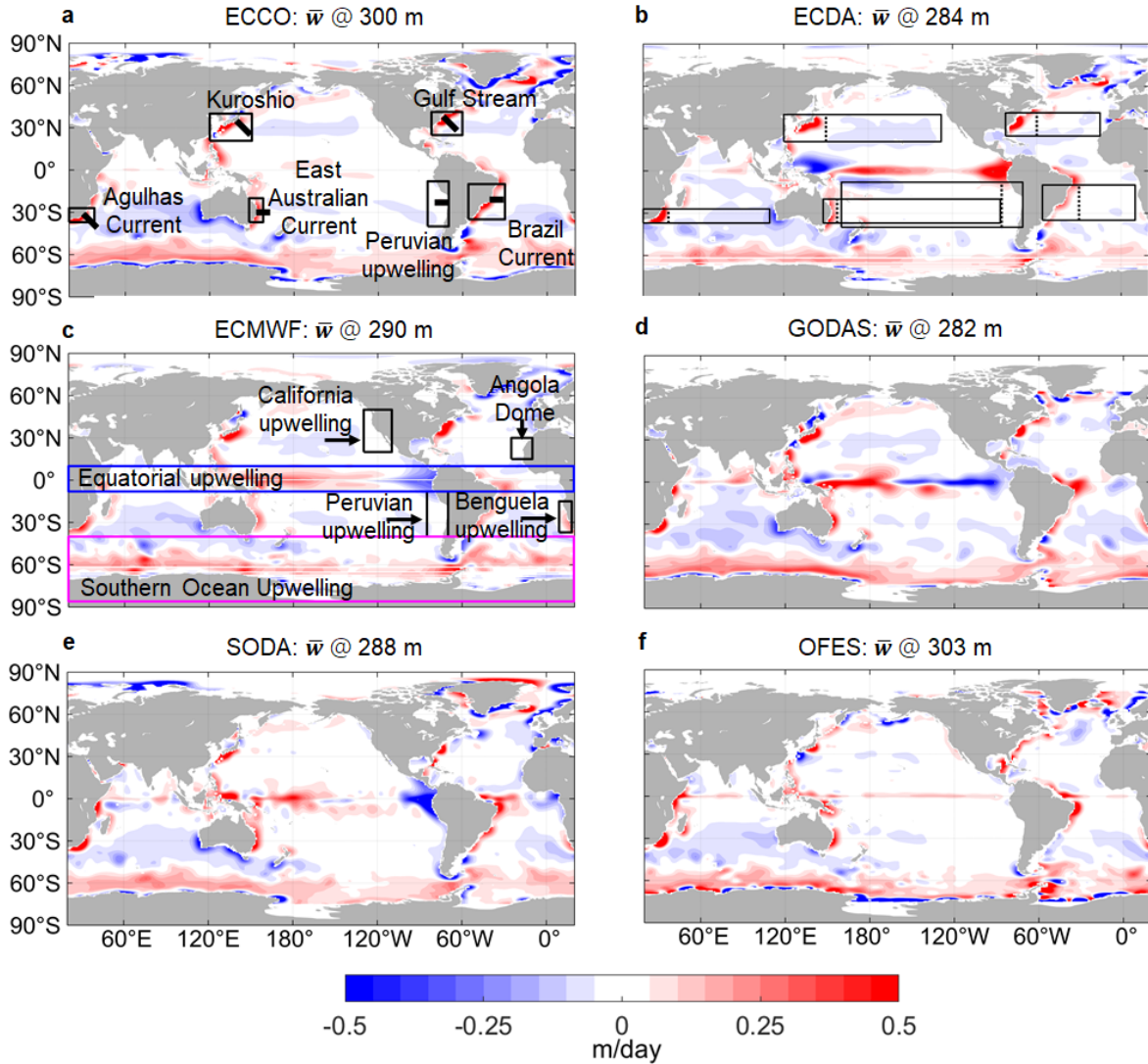
417 X.L. and Y.L. conceived the study. F.L. conducted the analyses. M.A.S. helped to develop the
418 mechanistic explanation. X.L. and F.L. drafted the manuscript. All authors discussed the results
419 and contributed to improving the manuscript.

420

421 **Competing interests**

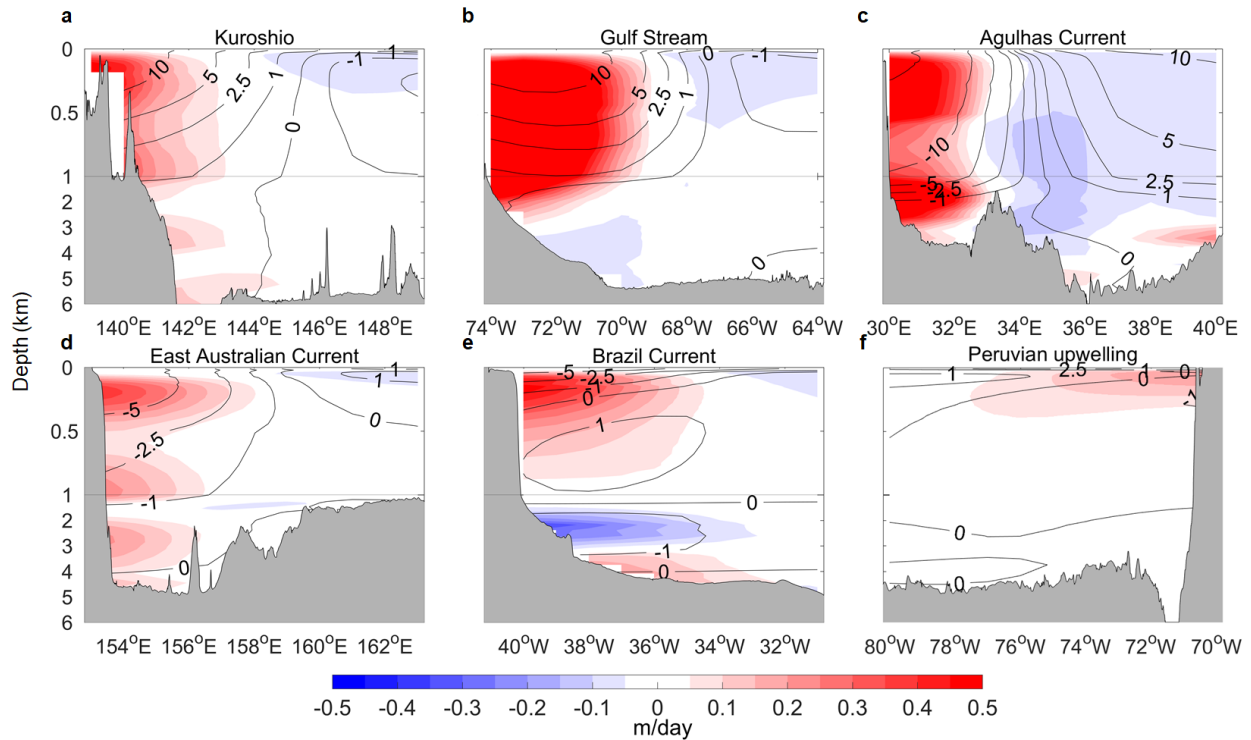
422 The authors declare no competing interests.

423



424

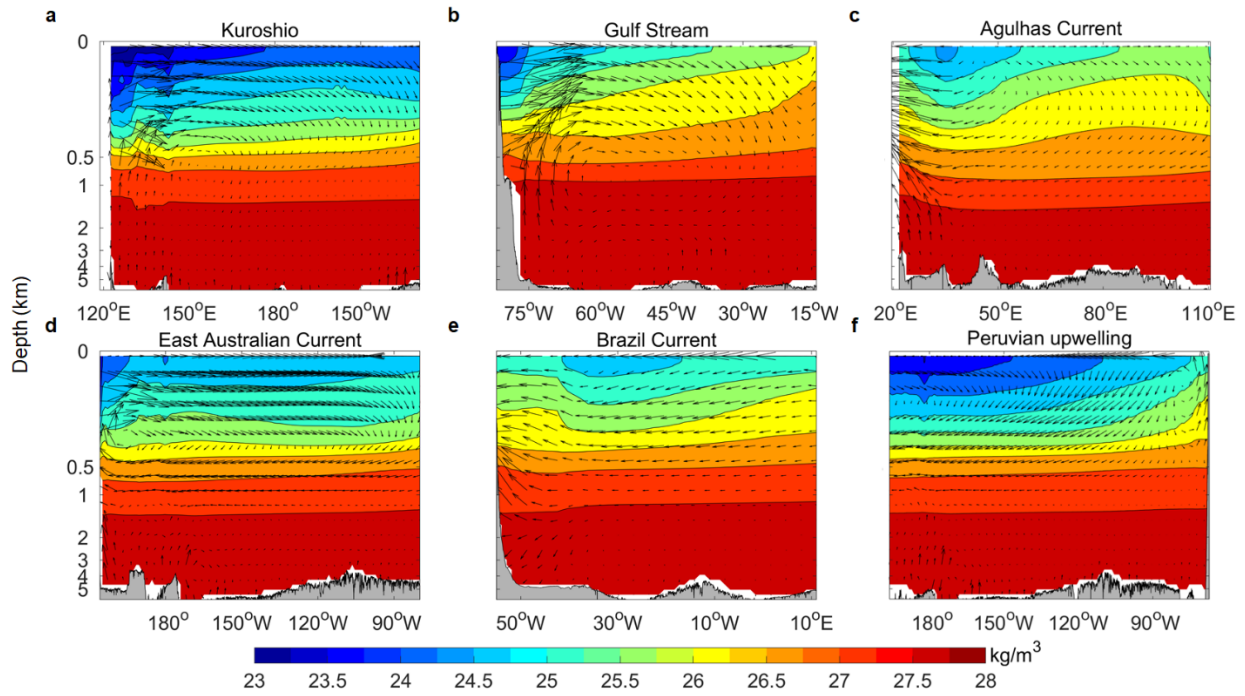
425 **Fig. 1** Time-averaged vertical velocity \bar{w} near 300 m between Jan 1992 and Dec 2009. \bar{w} from
 426 six selected products: **a** ECCO. **b** ECDA. **c** ECMWF. **d** GODAS. **e** SODA. **f** OFES. The black
 427 boxes in **a** show the domains of the five western boundary and one eastern boundary systems
 428 investigated in this study. The thick black lines represent the cross sections shown in Fig. 2. The
 429 black boxes in **b** (at the same latitude band of the corresponding boxes in **a**) represent the
 430 domains where vertical volume flux was calculated. The dashed lines roughly split the domains
 431 into WBC regions and the rest of the subtropical ocean basins. Boxes in **c** mark three other well-
 432 known upwelling regimes (equatorial, eastern boundary and the Southern Ocean).



433

434 **Fig. 2** Time-averaged vertical velocity \bar{w} (colour) and horizontal velocity (contour lines, unit:
 435 cm/s) in selected cross sections from ECCO. The other datasets show similar spatial patterns
 436 (Supplementary Figs. 3-8). The cross sections are marked with black lines in Fig. 1a. **a** Kuroshio.
 437 **b** Gulf Stream. **c** Agulhas Current. **d** East Australian Current. **e** Brazil Current. **f** Peruvian
 438 upwelling. The contour lines show the horizontal velocity (cm/s) perpendicular to the cross
 439 sections, indicative of the strength of adjacent western boundary currents. Note that the depth
 440 axis is stretched for better visualization.

441

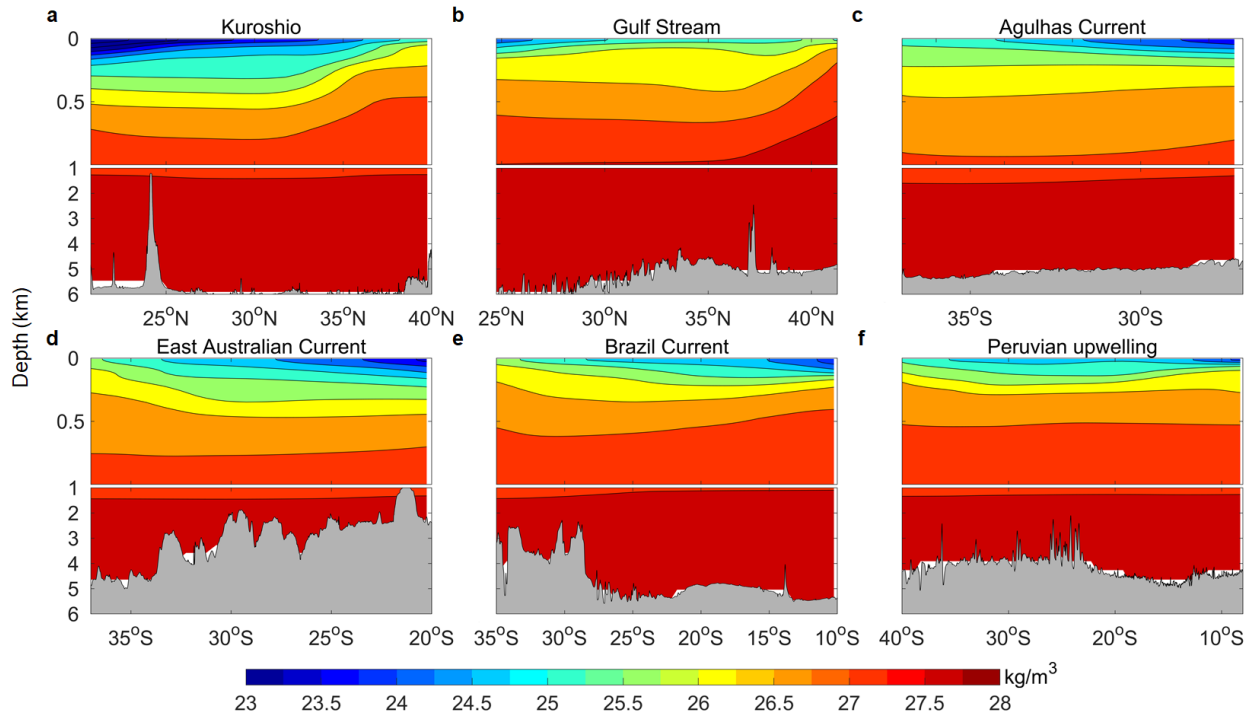


442

443 **Fig. 3** Meridional averages of the time-averaged current vector (arrows, normalized in each
 444 region individually for better visualization) and potential density anomaly (contours) in selected
 445 regions from ECCO. The other datasets show similar spatial patterns. The averaged regions,
 446 which are marked with black boxes in Fig. 1b, correspond to: **a** Kuroshio. **b** Gulf Stream. **c**
 447 Agulhas Current. **d** East Australian Current. **e** Brazil Current. **f** Peruvian upwelling.

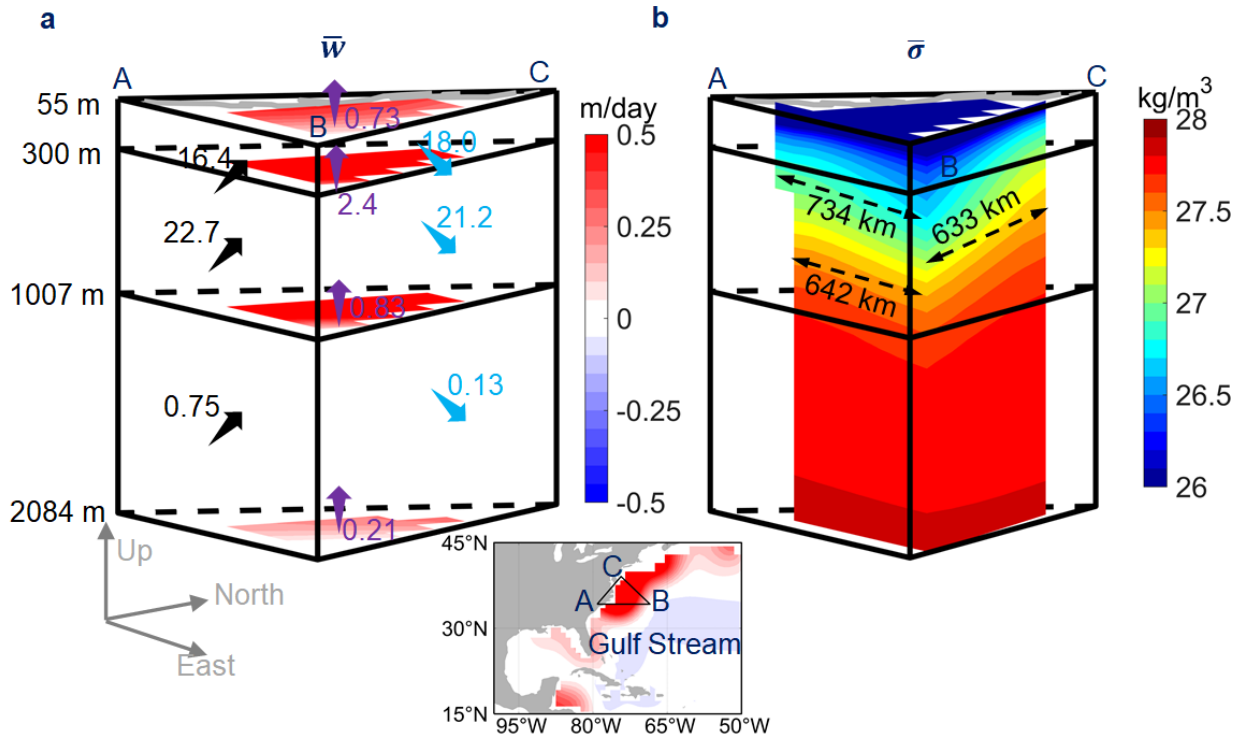
448

449



450

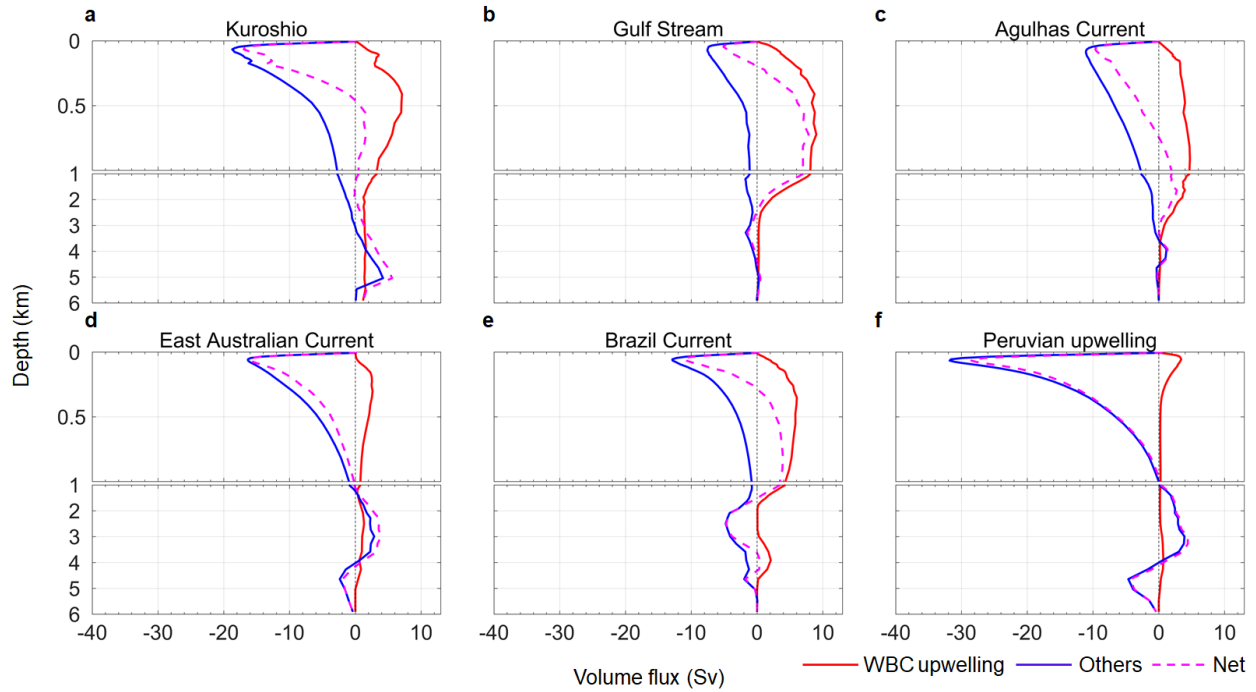
451 **Fig. 4** Potential density along the WBCs and Peruvian upwelling. The potential density
 452 anomalies were derived along the meridional direction of the WBC regions marked in Fig. 1. **a**
 453 Kuroshio. **b** Gulf Stream. **c** Agulhas Current. **d** East Australian Current. **e** Brazil Current. **f**
 454 Peruvian upwelling.



455

456 **Fig. 5** Time-averaged vertical velocity \bar{w} , potential density anomaly $\bar{\sigma}$, and volume flux in a
 457 triangle-shape domain in the Gulf Stream region. **a** Time-averaged vertical velocity at four
 458 depths (colours) and lateral and vertical volume fluxes. The black and blue arrows represent the
 459 lateral volume fluxes in Sv, and the purple arrows show the vertical volume fluxes in Sv. **b**
 460 Time-averaged potential density anomaly along the sections AB and BC of the triangle-shaped
 461 domain between 55 and 2000 m (shown in the inset). The grey curve in the 55 m section in **a**, **b**
 462 represents the coastline. The results are based on ECCO data on the native grids.

463



464

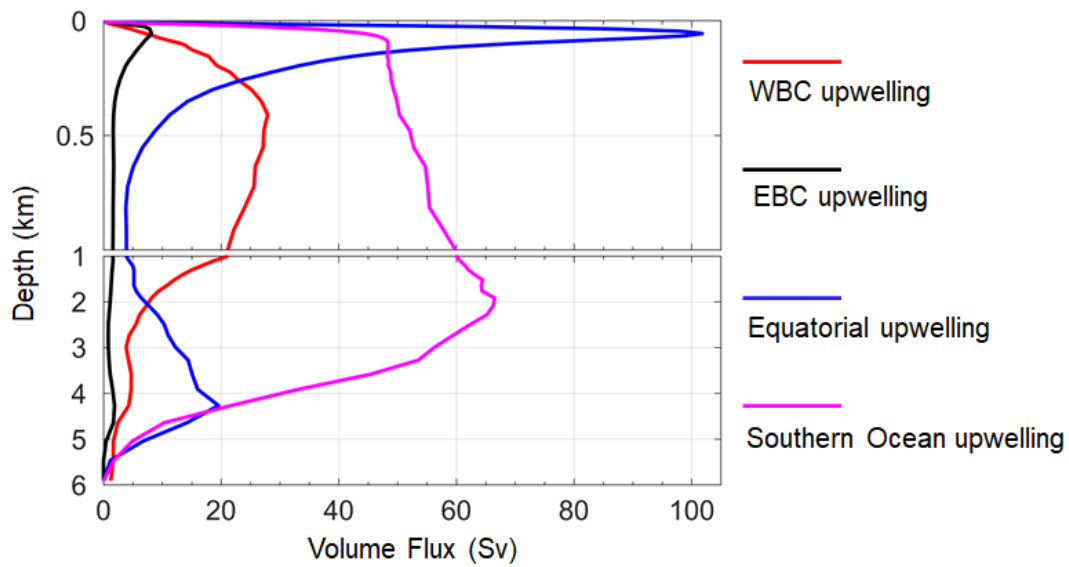
465 **Fig. 6** Vertical volume fluxes in the subtropical ocean basins from ECCO. Vertical volume
 466 transport due to the WBC upwelling is shown in red, vertical volume transport integrated across
 467 the rest of the corresponding ocean basin within the same latitude band is shown in blue, and the
 468 net vertical volume transport is displayed as the magenta dashed line. The six regions, which are
 469 marked in Fig. 1b, correspond to **a** Kuroshio. **b** Gulf Stream. **c** Agulhas Current. **d** East
 470 Australian Current. **e** Brazil Current. **f** Peruvian upwelling. Note that the depth axis is divided
 471 into two parts for better visualization.

472

473

474

475



476

477 **Fig. 7** Comparisons of vertical volume transport in four different upwelling regimes. The four
 478 regimes are WBCs, the Eastern Boundary Currents (EBC), the Equatorial region and the
 479 Southern Ocean. The vertical volume transport is calculated within the corresponding upwelling
 480 regions marked in Fig. 1c.

481

482

483

Supplementary Information for

484

485

Intense Subsurface Upwelling Associated with Major Western

486

Boundary Currents

487

488

Fanglou Liao¹, Xinfeng Liang^{1*}, Yun Li¹ & Michael Spall²

489

1. School of Marine Science and Policy, University of Delaware, Lewes, DE 19958, USA

490

2. Woods Hole Oceanographic Institution, Woods Hole, MA, 02543, USA

491

492

493

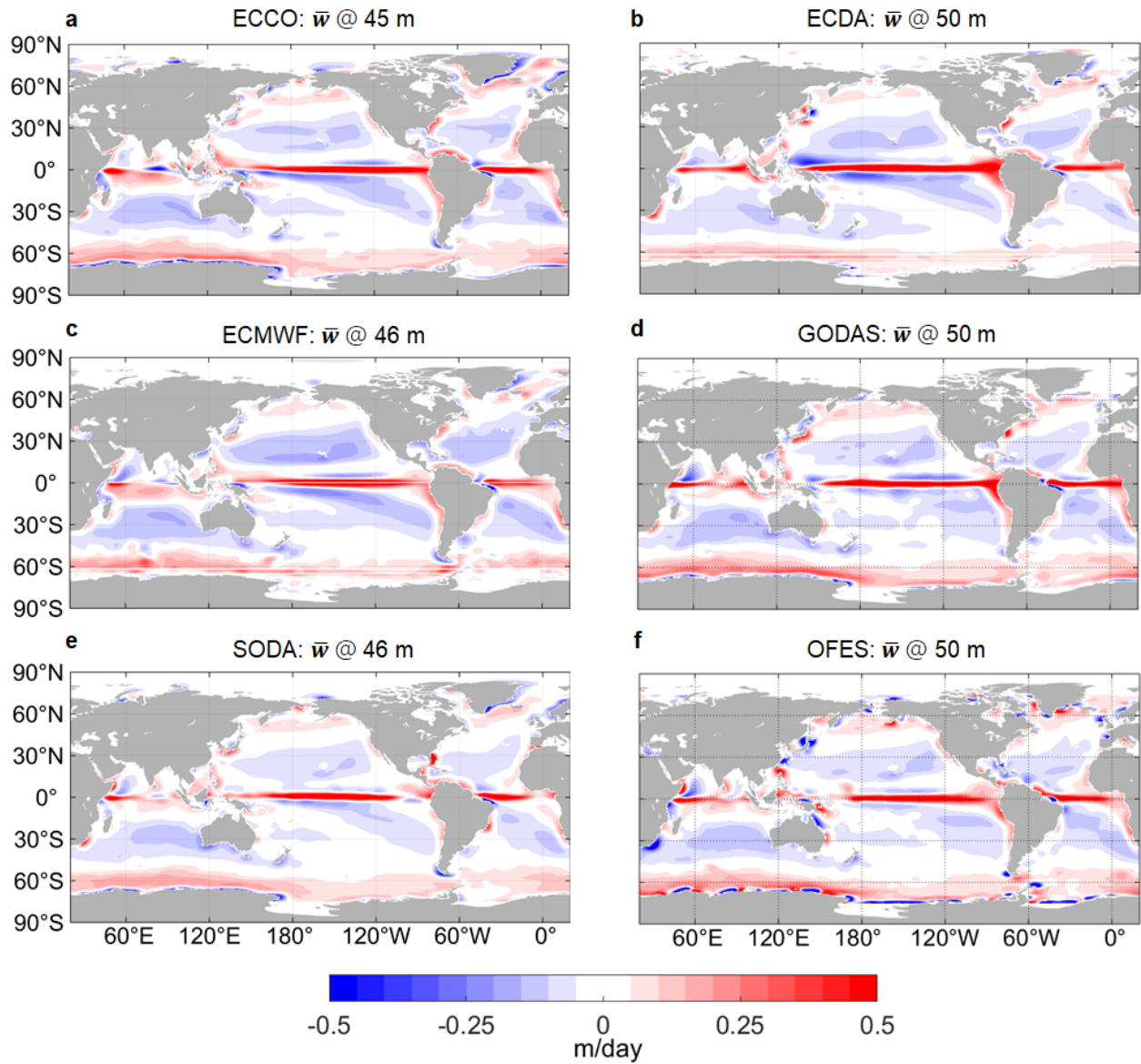
494

495

496

497

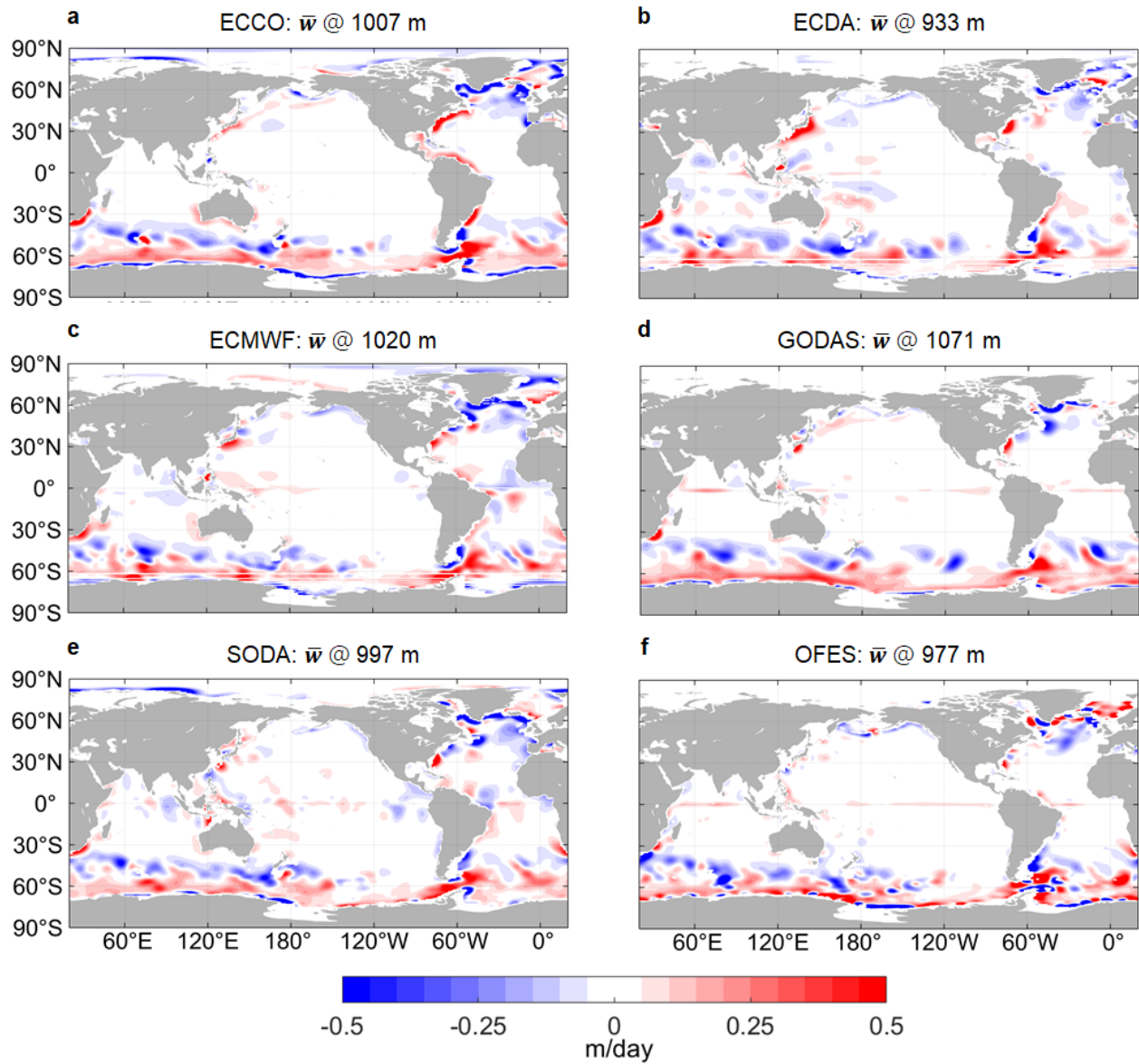
498



503 **Supplementary Fig. 1** Time-averaged vertical velocity \bar{w} at around 50 m. **a** ECCO. **b** ECDA. **c**
504 ECMWF. **d** GODAS. **e** SODA. **f** OFES.

505

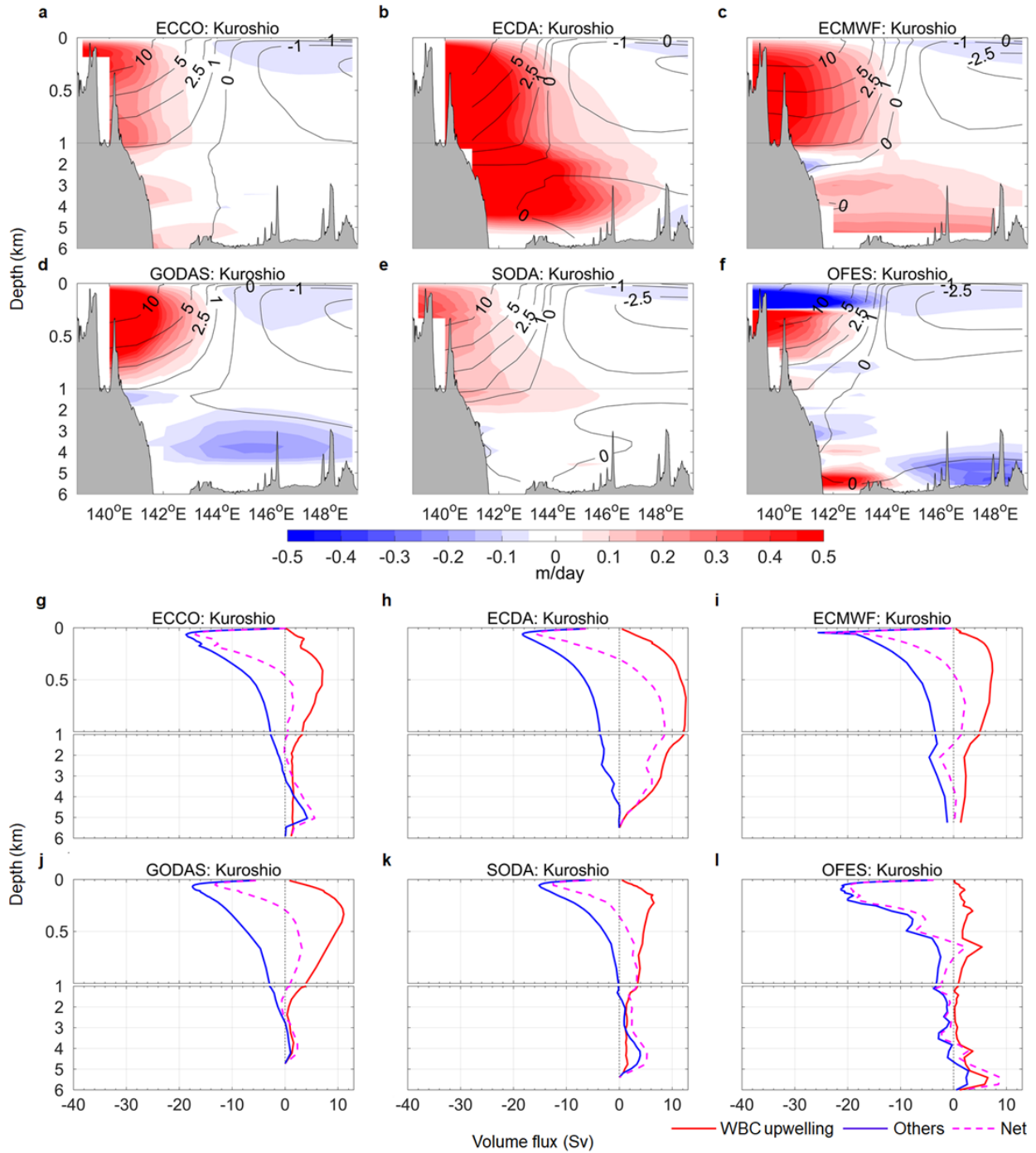
506



507

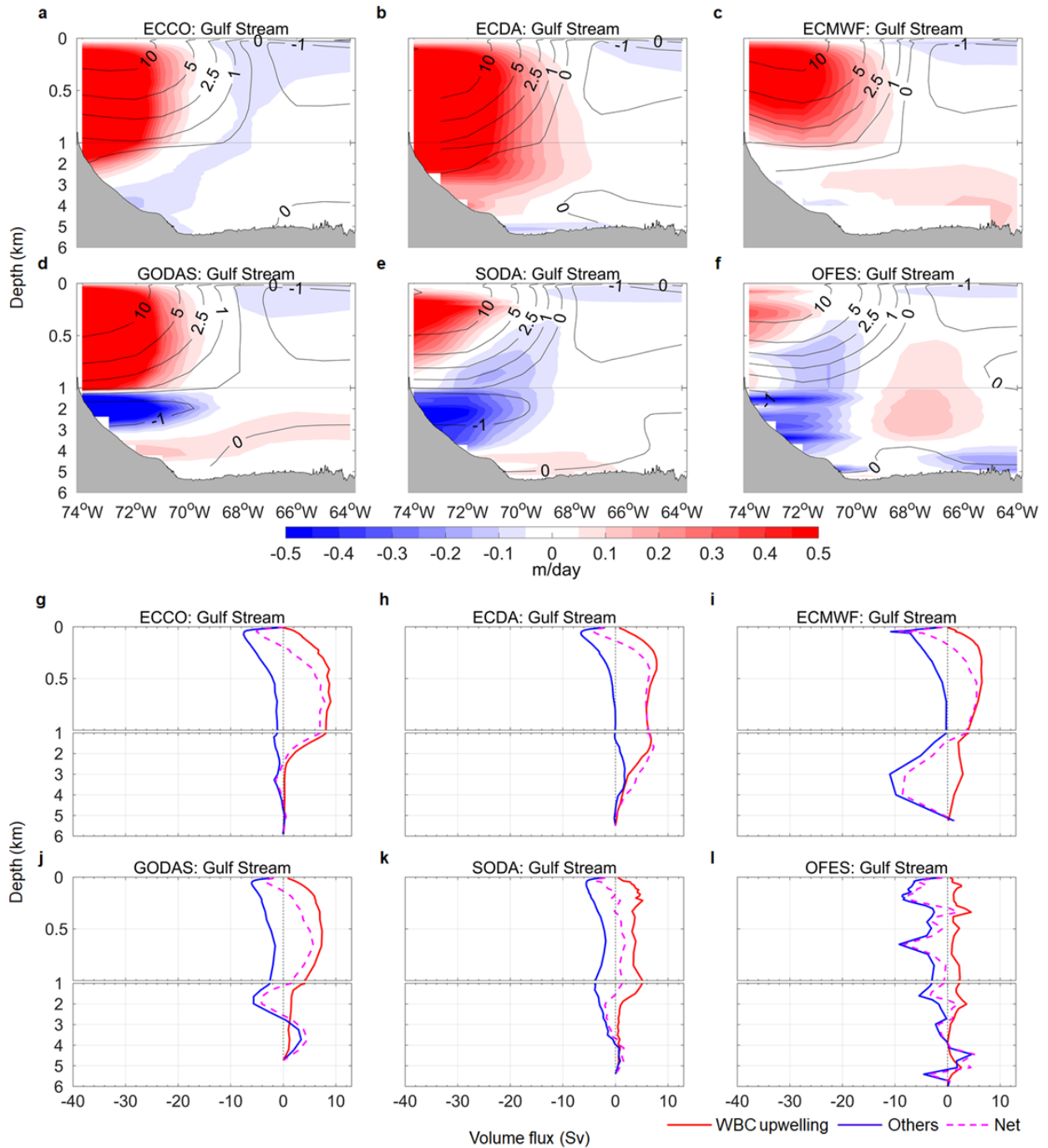
508 **Supplementary Fig. 2** Time-averaged vertical velocity \bar{w} at around 1000 m. **a** ECCO. **b** ECDA.

509 **c** ECMWF. **d** GODAS. **e** SODA. **f** OFES.



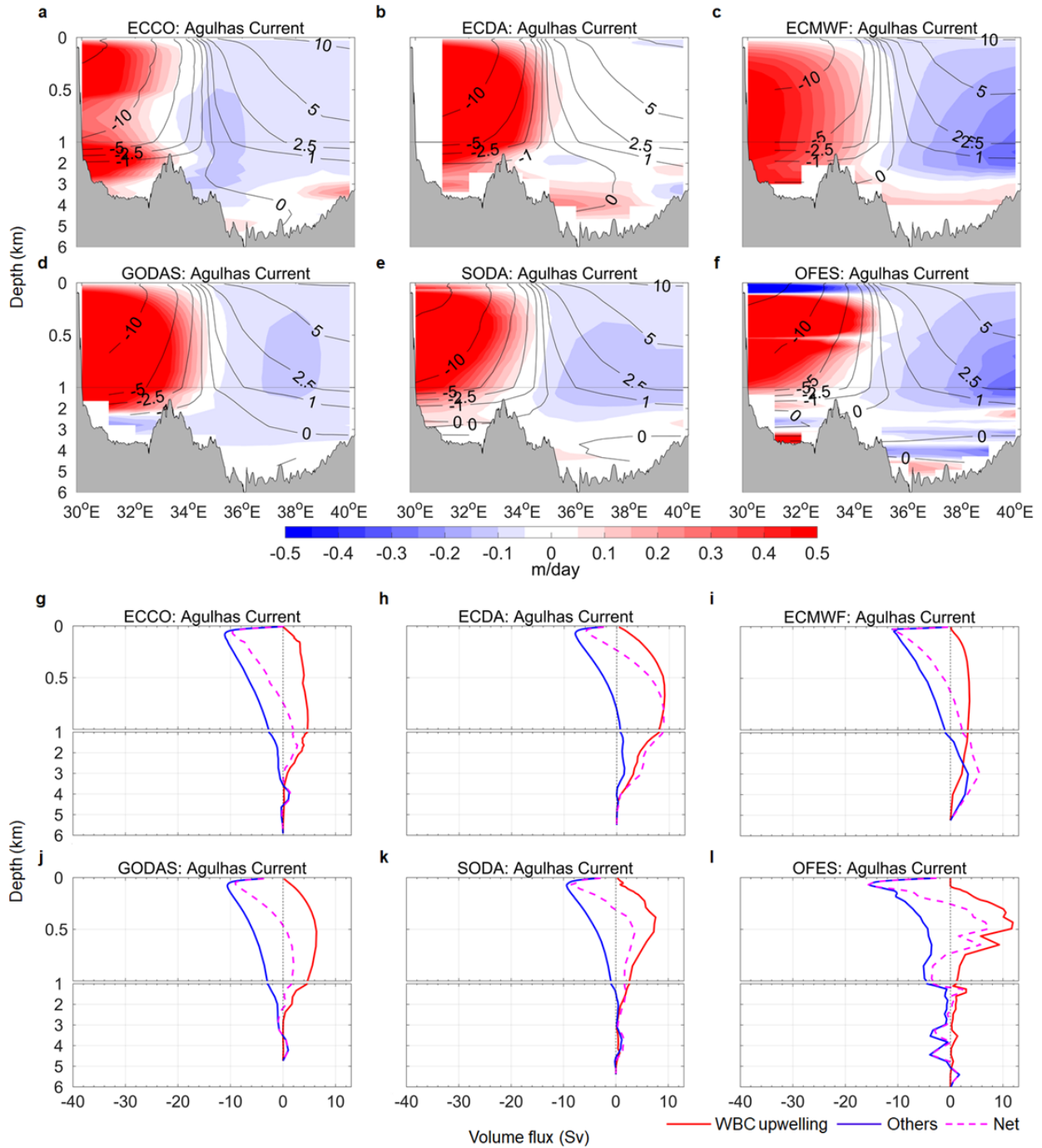
510

511 **Supplementary Fig. 3** Time-averaged vertical velocity \bar{w} (colour) along with horizontal speed
 512 distribution (contours, unit: cm/s) in selected cross sections (shown in Fig. 1a) and volume flux
 513 in the Kuroshio Current region. **a, g** ECCO. **b, h** ECDA. **c, i** ECMWF. **d, j** GODAS. **e, k** SODA.
 514 **f, l** OFES.



515

516 **Supplementary Fig. 4** Time-averaged vertical velocity \bar{w} (colour) along with horizontal speed
 517 distribution (contours, unit: cm/s) in cross sections (shown in Fig. 1a) and volume flux in the
 518 Gulf Stream region. **a, g** ECCO. **b, h** ECDA. **c, i** ECMWF. **d, j** GODAS. **e, k** SODA. **f, l** OFES.



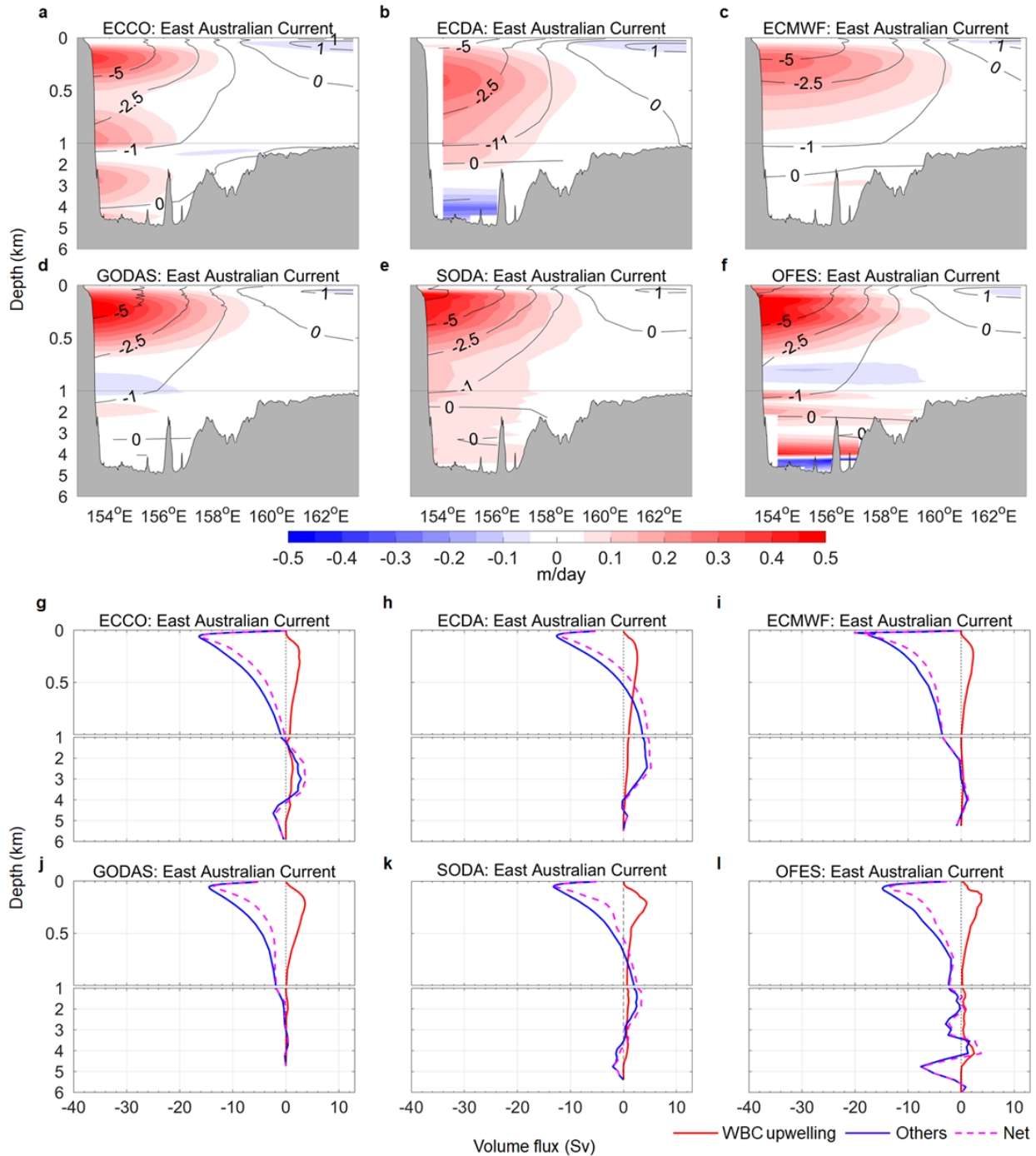
519

520 **Supplementary Fig. 5** Time-averaged vertical velocity \bar{w} (colour) along with horizontal speed

521 distribution (contours, unit: cm/s) in cross sections (shown in Fig. 1a) and volume flux in the

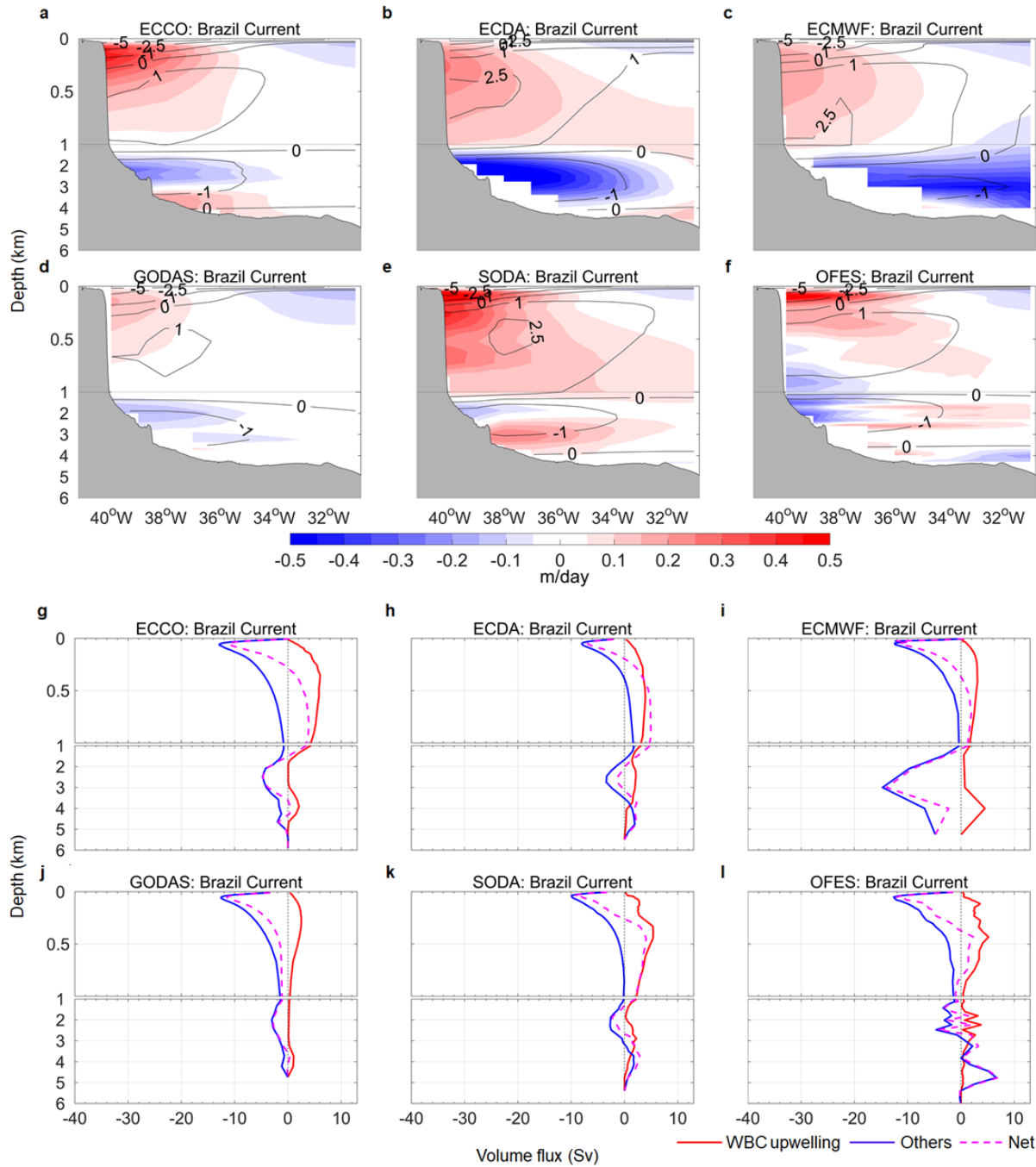
522 Agulhas Current region. **a, g** ECCO. **b, h** ECDA. **c, i** ECMWF. **d, j** GODAS. **e, k** SODA. **f, l**

523 OFES.



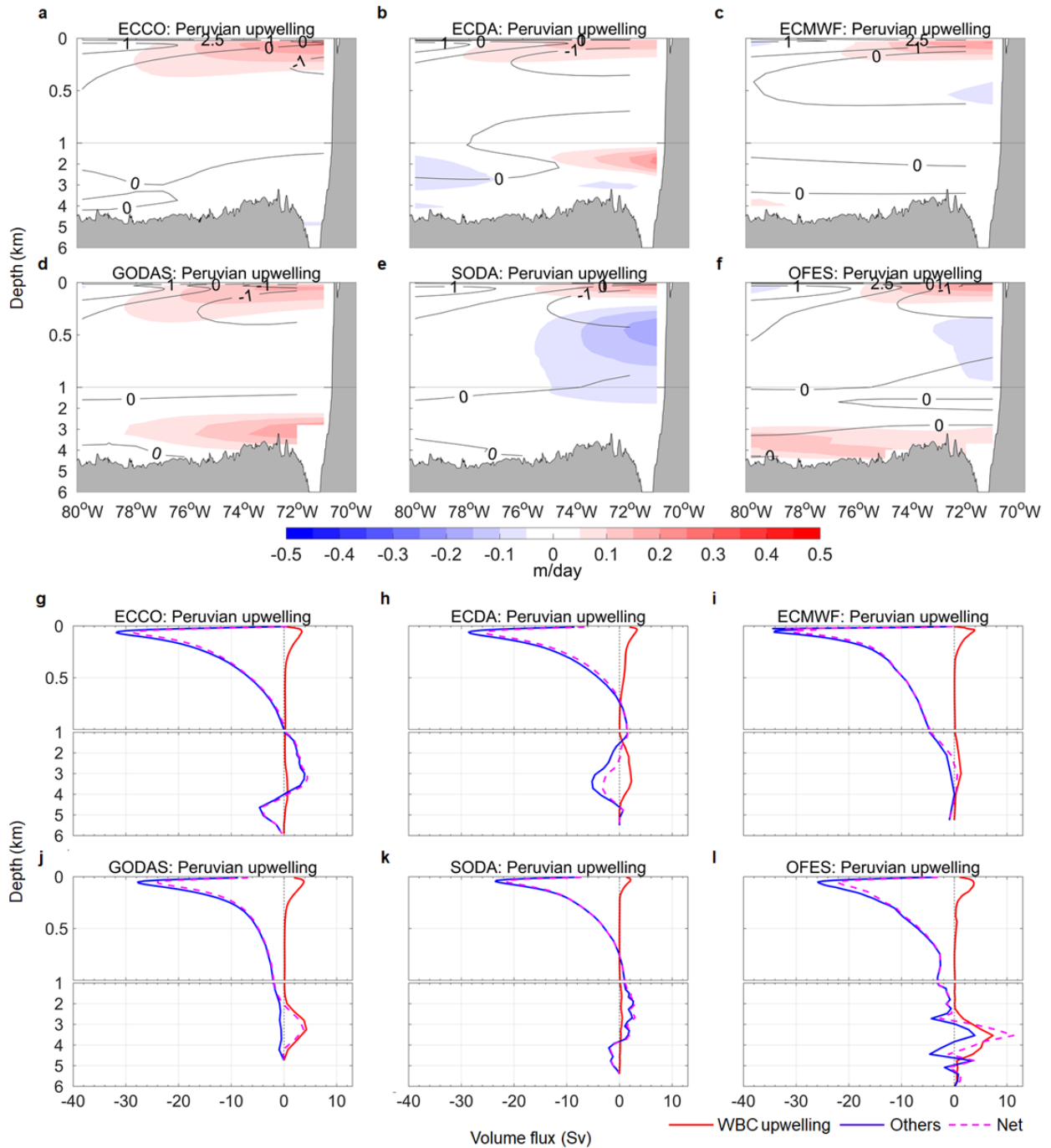
524

525 **Supplementary Fig. 6** Time-averaged vertical velocity \bar{w} (colour) along with horizontal speed
 526 distribution (contours, unit: cm/s) in cross sections (shown in Fig. 1a) and volume flux in the
 527 East Australian Current region. **a, g** ECCO. **b, h** ECDA. **c, i** ECMWF. **d, j** GODAS. **e, k** SODA.
 528 **f, l** OFES.



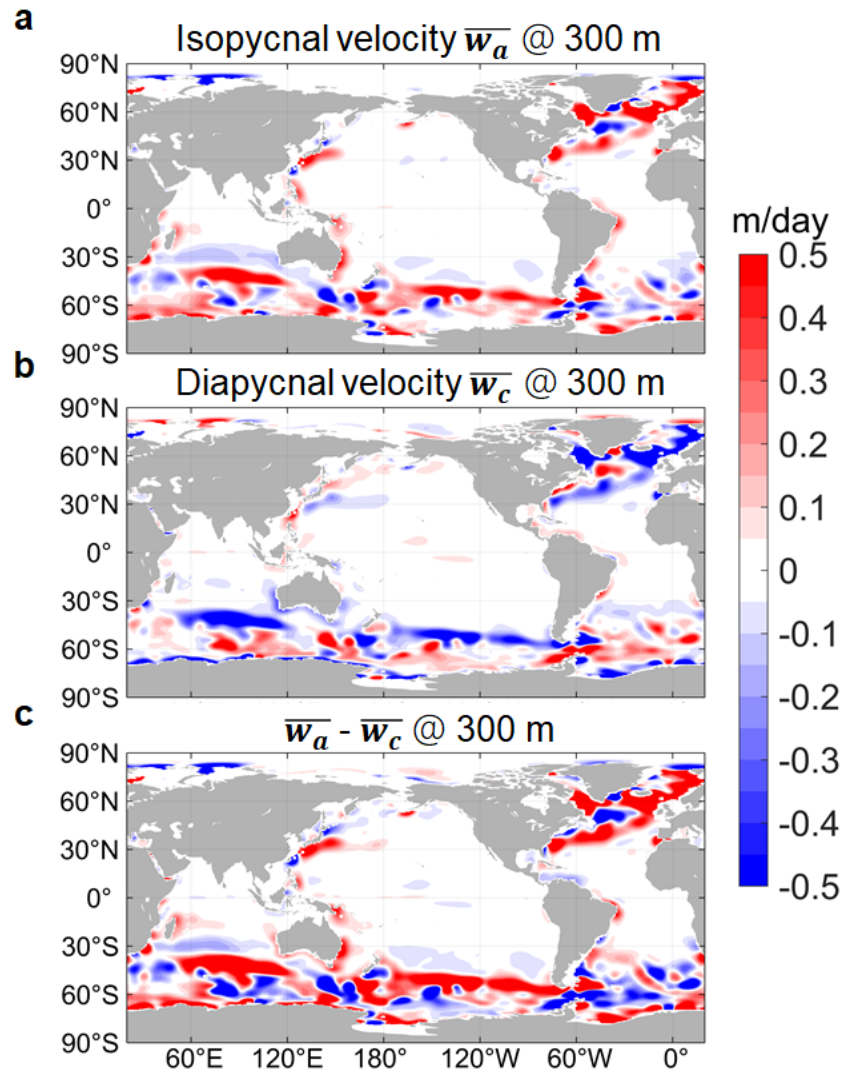
529

530 **Supplementary Fig. 7** Time-averaged vertical velocity \bar{w} (colour) along with horizontal speed
 531 distribution (contours, unit: cm/s) in cross sections (shown in Fig. 1a) and volume flux in the
 532 Brazil Current region. **a, g** ECCO. **b, h** ECDA. **c, i** ECMWF. **d, j** GODAS. **e, k** SODA. **f, l**
 533 OFES.



534

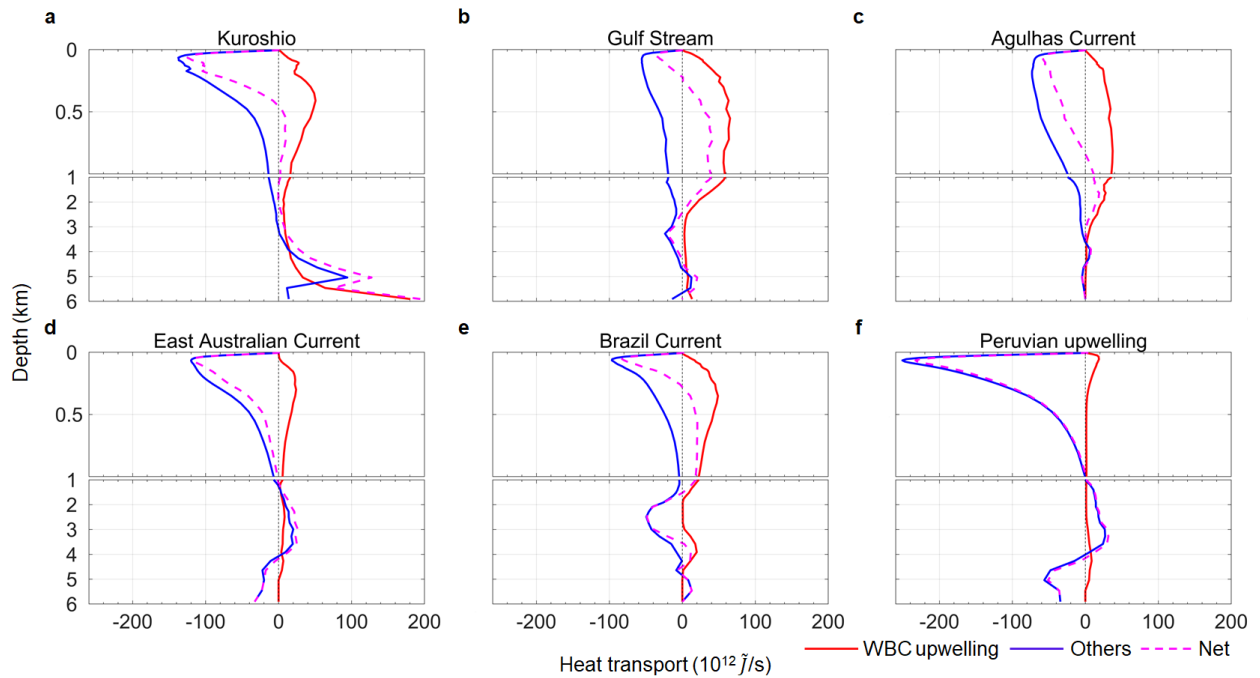
535 **Supplementary Fig. 8** Time-averaged vertical velocity \bar{w} (colour) along with horizontal speed
 536 distribution (contours, unit: cm/s) in cross sections (shown in Fig. 1a) and volume flux in the
 537 Peruvian upwelling region. **a, g** ECCO. **b, h** ECDA. **c, i** ECMWF. **d, j** GODAS. **e, k** SODA. **f, l**
 538 OFES.



539

540 **Supplementary Fig. 9** Along- and across-isopycnal components of the time-mean vertical
 541 velocity \overline{w} at around 300 m. **a** Isopycnal vertical velocity. **b** Diapycnal vertical velocity. **c**
 542 Differences between isopycnal and diapycnal vertical velocities. The results are based on ECCO.

543



544

545 **Supplementary Fig. 10** Vertical heat transport in the WBC regions and Peruvian upwelling

546 region. **a** Kuroshio. **b** Gulf Stream. **c** Agulhas Current. **d** East Australian Current. **e** Brazil

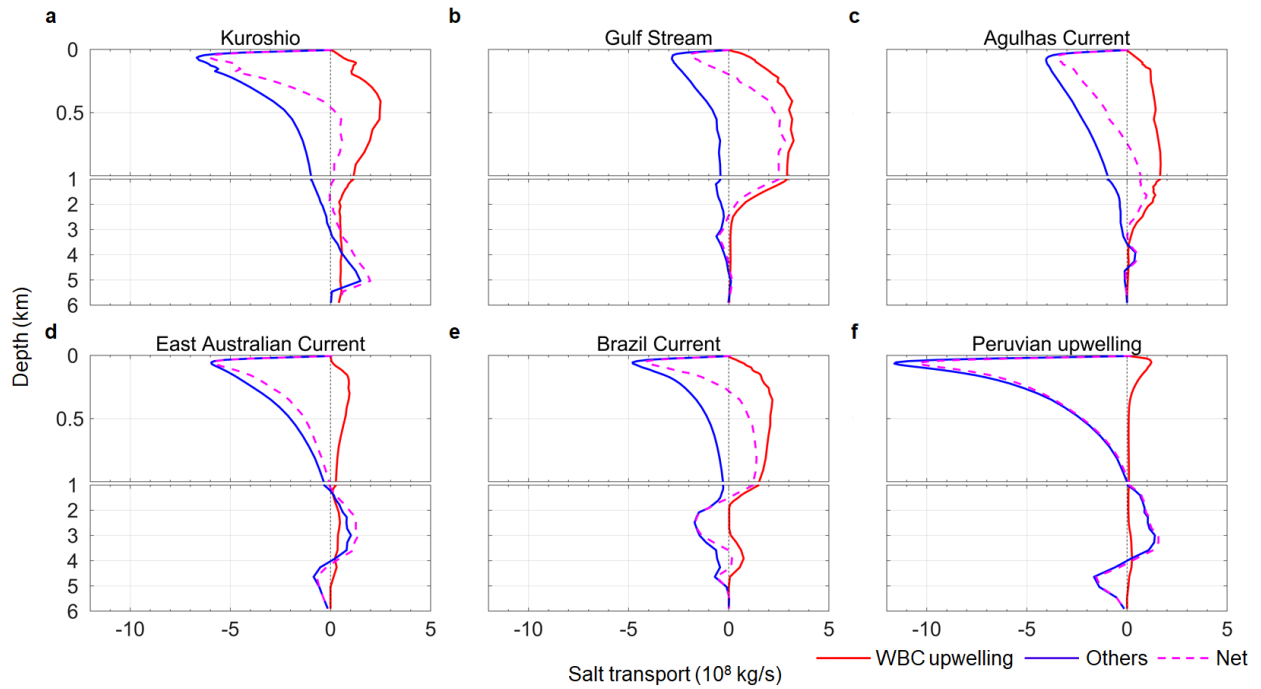
547 Current. **f** Peruvian upwelling. \tilde{j} means equivalent joules as we used normalized temperature at

548 each layer to calculate the heat flux. The results are based on ECCO.

549

550

551



552

553 **Supplementary Fig. 11** Vertical salt transport in the WBC regions and Peruvian upwelling

554 region. **a** Kuroshio. **b** Gulf Stream. **c** Agulhas Current. **d** East Australian Current. **e** Brazil

555 Current. **f** Peruvian upwelling. The results are based on ECCO.

556

557

558

559

560 **Supplementary Table**
 561

562 **Supplementary Table 1: Summary of the six ocean data products**

| Product | ECCO | ECDA | ECMWF | GODAS | SODA | OFES |
|------------------|--------------------------|-----------|-----------|-----------|-----------|-----------|
| Version | v4r3 | | ora-s3 | | 3.4.2 | |
| Model | MITgcm | MOM4 | HOPE | MOM3 | POP2 | MOM3 |
| Lon grids | 720 | 360 | 360 | 360 | 720 | 3600 |
| Lat grids | 360 | 200 | 179 | 418 | 330 | 1500 |
| Vertical grids | 50 (z*) | 50 (z) | 29 (z*) | 40 (z*) | 50 (z*) | 54 (z) |
| Assimilated data | T, S, SST, SSS, SSH, OBP | T, S, SST | T, S, SSH | T | T, S, SST | |
| Time span | 1992-2015 | 1961-2016 | 1959-2009 | 1980-2019 | 1980-2018 | 1950-2016 |

563 Lon means longitude; Lat means latitude; z in the vertical grid row means the vertical coordinate
 564 is in z level and z* means z-star level; T means temperature; S means salinity; SST means sea
 565 surface temperature; SSS means sea surface salinity; SSH means sea surface height; OBP means
 566 ocean bottom pressure.

567